High Vacuum Deposition of Biferrocene Thin Films on Room Temperature Substrates

Roland Leber,[1,3,4,5] Lucy E. Wilson,[2] Peter Robaschik,[1,5] Michael S. Inkpen,[2] David J. Payne,[1,5] Nicholas J. Long,[2] Tim Albrecht,[2] Cyrus F. Hirjibehedin[3,4,6] and Sandrine Heutz[1,5]*

AUTHOR ADDRESS

1) Department of Materials, Imperial College London, London, SW7 2AZ, UK

2) Department of Chemistry, Imperial College London, London, SW7 2AZ, UK

3) Department of Physics and Astronomy, University College London, London, WC1E 6BT, UK

4) London Centre for Nanotechnology, University College London London, WC1H 0AH, UK

5) London Centre for Nanotechnology, Imperial College London, London, SW7 2AZ, UK

6) Department of Chemistry, University College London (UCL), London, WC1H 0AJ, UK

ABSTRACT: Metallocenes are a promising candidate for future spintronic devices due to their versatile and tunable magnetic properties. However, single metallocenes, e. g. ferrocene, sublimate below room temperature and therefore the implementation for future applications is challenging. Here, a method to prepare biferrocene thin films using organic molecular beam deposition (OMBD) is presented, and the effect of substrate and deposition rate on the film structure and morphology as well as its chemical and magnetic properties is investigated. On Kapton and Si substrates, biferrocene interacts only weakly with the substrate and distinct grains scattered over the surface are observed. By incorporating a 3,4,9,10-perylenetetracarboxylic dianhydride (PTCDA) seeding layer and depositing biferrocene at high deposition rates of 1.0 Å s^{-1}, it is possible to achieve a well-ordered densely packed film. With spintronic applications in mind, the magnetic properties of the thin films are characterized using superconducting quantum interference magnetometry (SQUID). Whereas initial SQUID measurements show weak ferromagnetic behaviour up to room temperature due to oxidized molecule fragments, measurements of biferrocene on PTCDA capped with LiF show the diamagnetic behaviour expected of biferrocene. Through the successful deposition of biferrocene thin films and the ability to control the spin state, these results demonstrate a first step towards metallocene-based spintronics.

1. Introduction

With the first synthesis of ferrocene in the early 1950s by Kealy and Pauson,[1] and independently by Miller, Tebboth and Tremaine[2] a new class of molecules was born. The family of metallocenes quickly grew and now includes a vast number of bis(η5-cyclopentadienyl)-metal molecules, containing different 3d metals like iron, nickel, and cobalt as well as 4d and 5d metals like ruthenium and osmium. Furthermore, it is possible to link metallocene monomers via covalent bonds to form open chains of nearly arbitrary length and even closed structures such as rings.[3] Therefore, metallocene species are ideal systems in which to study inter-metal interactions.[4]

Initially, metallocenes were thoroughly studied for their diverse properties in redox reactions, chemical catalysis and as precursors for metal-based structures thanks to easy release of the cyclopentadienyl rings[5]. In addition, metallocene dimers such as biferrocene generated great interest due to their mixed valence properties after oxidation.[6]

More recently, a broader range of applications of metallocenes have been identified, including lowering the work function of electrodes in the context of organic electronics[7, 8] or facilitating the production of aligned carbon nanotubes via pyrolysis.[9, 10]

By changing the metal centre, linking multiple/different metallocenes, adding ligands or oxidation of the molecules, different magnetic properties can be achieved. One especially prominent example is the decamethylbimetallocenes family, which exhibits diamagnetic behaviour with the metal being Fe^{2+} or Co^{3+} (oxidized using PF_6), ferromagnetic coupling in the case of Co^{2+} and antiferromagnetic coupling in the case of V^{2+} and Ni^{2+}.[11, 12]

Special interest in metallocenes arose within the field of spintronics after theoretical studies showed that ferrocene wires possess the ability to generate a nearly 100% spin-polarized current.[13] Furthermore, theoretical studies conducted on bicobaltocene and binickelocene showed spin-filtering properties,[14] and current rectification is predicted for nickelocenylferrocene.[15] Simulations carried out on ferrocene deposited on pristine graphene nanoribbons showed a possible spin valve structure that could generate a perfect magnetoresistive effect.[16] Furthermore, using STM it was demonstrated that nickelocene maintains its spin on metallic surfaces.[17] Hence, metallocenes are promising candidates for the realisation of future organic spintronic devices and quantum computing. However, a major challenge in utilising metallocenes in future spintronic devices is the capability to deposit them as stable thin films. For example, ferrocene sublimates below room temperature.[18]

In this work, we report the successful deposition and characterisation of biferrocene (Fc_2) thin films on various substrates. In contrast to ferrocene, biferrocene has a significantly higher sublimation temperature due to its larger molecular mass. Subsequent analysis of the films using atomic force microscopy (AFM) and scanning electron microscopy (SEM) showed distinct grains scattered over the surface due to weak interactions with the Si and Kapton substrate. Well-ordered densely packed films were observed by depositing on a 3,4,9,10-perylenetetracarboxylic dianhydride (PTCDA) seeding layer and using high deposition rates. Initial superconducting quantum interference device (SQUID) measurements showed weak ferromagnetic behaviour, which in conjunction with X-ray photoelectron spectroscopy (XPS) measurements was attributed to oxidized molecular fragments. It is possible to suppress this ferromagnetism and observe the expected diamagnetic behaviour by using PTCDA as a seeding layer and LiF as a capping layer. With the ability to control the spin state of bimetallocene molecules via oxidation and selecting the magnetic properties via a suitable choice of the metal centre, the successful deposition of biferrocene molecules shows great potential towards metallocene-based spintronic devices.

2. Experimental Section

All depositions were carried out in a SPECTROS® organic molecular beam deposition (OMBD) system by Kurt J. Lesker® with a base pressure of around 5 x 10^{-7} mbar. Multilayer structures were grown without breaking vacuum. A targeted biferrocene film thickness as measured with a quartz crystal microbalance of 200 nm on PTCDA was chosen for all samples; however, depending on the substrate the achieved thickness varied due to a difference in the sticking coefficients. The nominal deposition rate was 0.1 and 1.0 Å s^{-1}. During deposition, the substrates were kept at room temperature and a sublimation temperature of 75-105 °C was used for the biferrocene molecules.

The XRD patterns were collected on a Philips X'Pert PRO PANalytical θ/2θ system using 40 kV source voltage and 40 mA source current (Cu-Kα, 0.154 nm). For sample imaging a Bruker Dimension Icon® AFM was used in Peak Force Tapping® mode as well as a ZEISS Leo Gemini 1525 SEM. Gwyddion software was used for detailed analysis of the AFM images. To get accurate values for coverage and film thickness, values were averaged over three 50 x 50 µm AFM images; the error bars are given by the standard deviation of the three images. The thin film thickness equivalent was calculated via the total grain volume averaged over three 50 x 50 µm images. The SEM imaging was carried out using a beam energy of 5 keV and the in-lens detector; a 10 nm Cr coating was applied directly prior to imaging. For chemical characterisation, Raman and XPS were measured on a Renishaw® inVia Raman microscope using an excitation wavelength of 532 nm and on a Thermo Scientific™ K-Alpha™+ XPS using an Al Kα X-ray source (hν = 1486.6 eV) and a 180° double focusing hemispherical analyser with a 2D detector, respectively. The XPS data was collected using a pass energy of 20 eV and an X-ray spot size of 400 µm. During all XPS measurements, a flood gun emitting low energy electrons and argon ions was used for charge compensation. The SQUID measurements were performed on a Quantum Design® MPMS-7 instrument. The samples for the SQUID measurements were prepared by depositing a 4 x 90 mm² strip of biferrocene on a 160 x 90 mm² sheet of Kapton/PTCDA on Kapton and subsequently rolled up and inserted in a plastic straw for the measurement. In this way, the background signal of the substrate can be eliminated. This method is explained in more detail elsewhere.[19]

Biferrocene synthesis:

General: Reactions were adapted from reported work which is referenced in the text. All reactions were performed using standard air sensitive chemistry and Schlenk line techniques under an atmosphere of nitrogen. No special precautions were taken to exclude air during the work-up. Solvents used in reactions were collected from solvent towers sparged with nitrogen and dried with 3 Å molecular sieves, apart from N-methyl-2-pyrrolidone (NMP), which was purchased as anhydrous (99.5%). Copper(I)thiophene-2-carboxylate (CuTC)[20] was synthesized using literature procedures. All other compounds were purchased from commercial suppliers and used without further purification. ^1H and $^{13}C\{^1H\}$ NMR spectra were recorded on a Bruker Avance 400 MHz spectrometer and referenced to the residual solvent peaks of $CDCl_3$ at 7.26 and 77.16 ppm. Coupling constants are measured in Hz. Mass spectrometry analyses were conducted by Lisa Haigh of the Mass Spectrometry Service, Imperial College London. Microanalyses were carried out at the Science Centre, London Metropolitan University, by Stephen Boyer using a Thermo Scientific (Carlo Erba) Flash 2000 Organic Elemental Analyser, configured for %CHN.

Synthesis of Iodoferrocene[21]

Ferrocene (10 g, 53.76 mmol) and KtBuO (750 mg, 6.68 mmol) were combined under an N_2 environment. Dry THF (500 ml) was added and the reaction flask was cooled to -78 °C. 1.9 M ^tBuLi solution in pentane (56 ml,

107.66 mmol) was added slowly to the solution and stirred for a further 2 hrs at -78 °C. Iodine (20 g, 78.80 mmol) was added as a solid against a flow of N_2 and the reaction was stirred for a further 30 min at -78 °C. The reaction was then allowed to warm to room temperature and quenched with water (1000 ml). The product was extracted into DCM (2 x 60 ml), washed with sodium thiosulphate solution and the solvent was removed to leave a brown oil. This was dissolved in n-hexane (500 ml) and washed with 0.2 M aqueous solution of $FeCl_3$ until the ^{1}H NMR showed the removal of ferrocene. The solution was then washed with water (3 x 100 ml), dried with $MgSO_4$, filtered and the solvent removed. The product was further purified by filtration through silica eluted with n-hexane and dried to yield an orange oil (13.26 g, 79%). ^{1}H NMR (400 MHz, CDCl$_3$): δ 4.41 (t, ^{3}JH-H =1.8, 2H), 4.19 (s, 5H), 4.15 (t, ^{3}JH-H =1.8, 2H) ^{13}C {1H} NMR (400 MHz, CDCl$_3$): δ 74.6 (2C), 71.2 (5C), 68.9 (2C), 39.9 (1C), MS ES+: m/z 99.1, ([M]+ Calc.: 399.1) (Found: C, 38.70; H, 3.12. Calc. for $C_{10}H_9FeI$ C, 38.51; H, 2.91.)

Synthesis of Biferrocene[2]

Iodoferrocene (4.89 g, 15.7 mmol), copper(I) thiophene-2-carboxylate (8.97 g, 47.1 mmol) and NMP (100 ml) were combined under N_2 and stirred overnight. The solution was filtered through alumina (V) with ethyl acetate (100 ml), washed with brine (5 x 100 ml) and dried over $MgSO_4$. This was filtered and the solvent removed. The product was purified through column chromatography eluted with n-hexane/DCM [1:0]→ [0:1] to yield the product as a red solid. (450 mg, 16.6%) ^{1}H NMR (400 MHz, CDCl$_3$): δ 4.35 (t, ^{3}JH-H =1.9, 2H), 4.17 (t, ^{3}JH-H =1.9, 2H), 3.99 (s, 5H) ^{13}C {1H} NMR (400 MHz, CDCl$_3$): δ 84.08 (2C), 69.31 (10C), 67.74 (4C), 66.52 (4C), MS ES+: m/z 370.0, ([M]+ Calc.: 370.0) (Found: C, 64.83; H, 4.98. Calc. for $C_{20}H_{18}Fe_2$ C, 64.91; H, 4.90.)
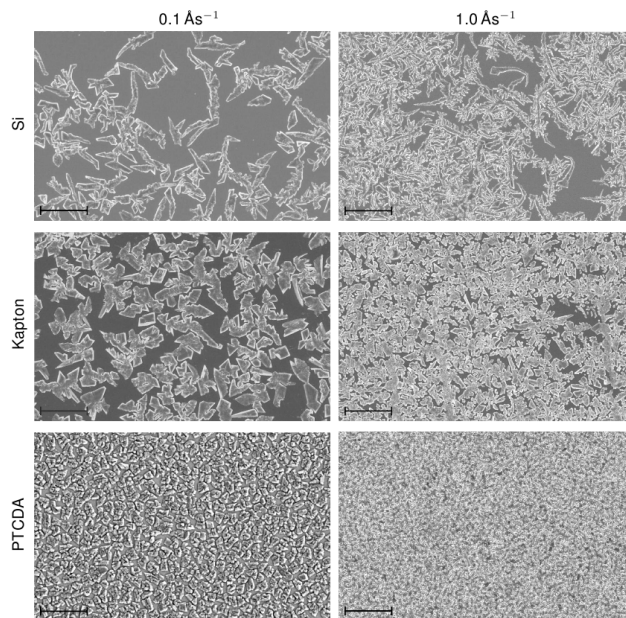
3. Results and Discussion

Figure 1 SEM images of 200 nm biferrocene on different substrates deposited with deposition rates of 0.1 and 1.0 Å s^{-1}; the scale bar equals 10 μm.

The morphology and structure of biferrocene thin films was investigated on Si, Kapton and PTCDA substrates. Figure 1 shows SEM survey images of biferrocene deposited with nominal deposition rates of 0.1 and 1.0 Å s^{-1} on the different substrates, up to a nominal film thickness of 200 nm.

Starting with the lower deposition rate, biferrocene molecules formed grains on the surface with the grain shape and size depending on the nature of the substrate. The grains on Si are more elongated in shape with large uncovered areas in between whereas the grains on Kapton are more triangular in shape separated by smaller uncovered areas. On Si and Kapton the nucleation density of the biferrocene molecules was low with a coverage of 30 ± 13% and 42 ± 2%, respectively; the coverage on Si varies more strongly than the coverage on the Kapton substrate. The actual film thickness calculated using the total grain volume for biferrocene on Si and Kapton was determined as 73 ± 33 nm and 161 ± 12 nm, respectively.

To improve the film coverage and morphology, PTCDA - a molecule known for forming π-π[22] or dipolar[23] interactions with other organic molecules - was chosen as a seeding layer. By growing biferrocene thin films on PTCDA, it was possible to increase the film coverage to 70 ± 2% and the film thickness equivalent (defined in experimental section) to 215 ± 10 nm. Furthermore, denser and more regularly shaped grains were observed due to the high nucleation density and limited space for the grains to grow laterally in comparison to the widely-spaced grains on Si and Kapton.
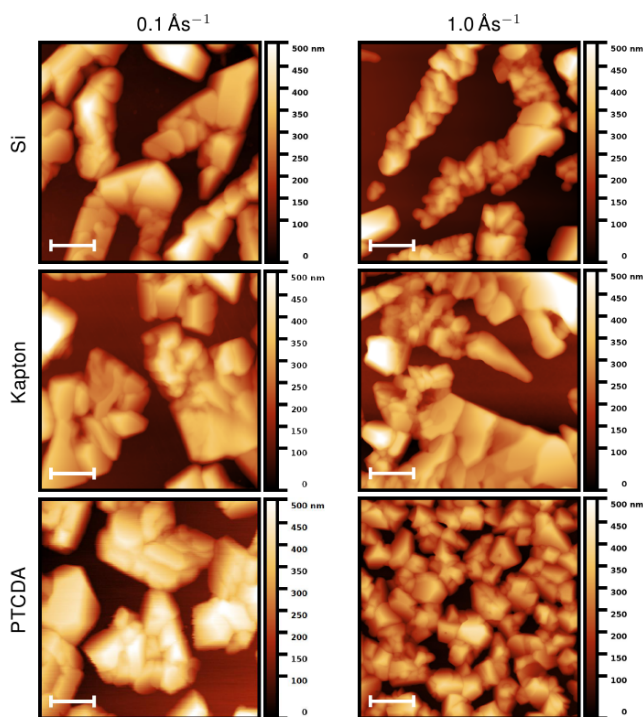
Figure 2 AFM images of nominal 200 nm biferrocene on different substrates deposited with deposition rates of 0.1 and 1.0 Å s⁻¹; the scale bar equals 1 µm.

Individual grains were studied in more detail using AFM (Figure 2). On all substrates, it was observed that the grains consist of multiple smaller crystals. Based on the substrate dependence of the grain shape and the grains being well separated with no evidence of a continuous wetting layer underneath, we suggest a Volmer-Weber island like growth mode indicating strong inter-molecular coupling.
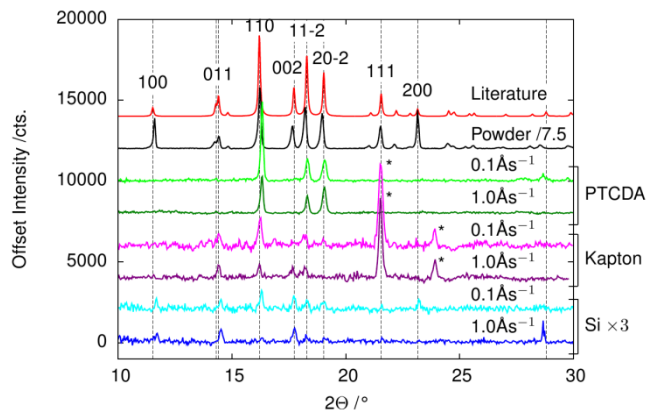

Figure 3 XRD pattern of biferrocene thin films on PTCDA/Si, Kapton and Si compared to the literature;[24] peaks marked with a "*" correspond to the Kapton substrate.

The crystal structure was studied using XRD, as shown in Figure 3. Powder measurements were similar to those previously obtained for biferrocene measured on a single crystal[24] with slightly different peak intensity ratios, which may be caused by an anisotropic grain shape of the powder resulting in preferential alignment of the grains relative to each other. On all substrates investigated, biferrocene

crystals showed diffraction from the (110), (11-2) and (20-2) planes; the films on all substrates except PTCDA on Si also adopted a (011) orientation. The molecular orientations relative to these planes are shown in Figure 4. Note that the biferrocene unit cell contains two inequivalent molecules oriented nearly perpendicular to each other with an angle of 87.6°;[24] therefore, it is not possible to achieve a packing with the cyclopentadienyl rings flat or perpendicular to the substrate. The dominant peak for biferrocene films on Kapton, Si, PTCDA and powder, as well as in prior measurements on single crystals[24] was at approximately 2θ = 16.2° corresponding to the (110) plane. In this configuration, the molecules are oriented at an angle of 87.2° and 22.7° relative to the crystal plane/substrate. To compare peak intensities between different samples, we used the texture factor[25] ζ to normalize the measured peak intensities ι relative to the intensities reported in literature for the biferrocene single crystal τ:

$$\zeta = \frac{\iota/\sum \iota}{\tau/\sum \tau}$$

The texture factor corresponding to the (110) plane in the case of biferrocene on PTCDA is the highest with 3.28 compared to 2.10 on Kapton, 1.63 on Cu and 1.16 on Si. This suggests a higher crystal alignment of biferrocene on PTCDA compared to the other substrates. Furthermore, Si was the only substrate with crystals oriented along the (200) plane. Based on the molecular alignment relative to the substrate for the (011), (110), (11-2) and (20-2) orientations, we conclude that the molecules interact with the substrate via hydrogen bonds. Therefore, the crystal orientations on PTCDA are quite surprising since PTCDA is known for forming π-π interactions[22] with aromatic molecules. However, biferrocene shows a similar behaviour as TCNQ by interacting with the PTCDA via hydrogen bonds.[19]
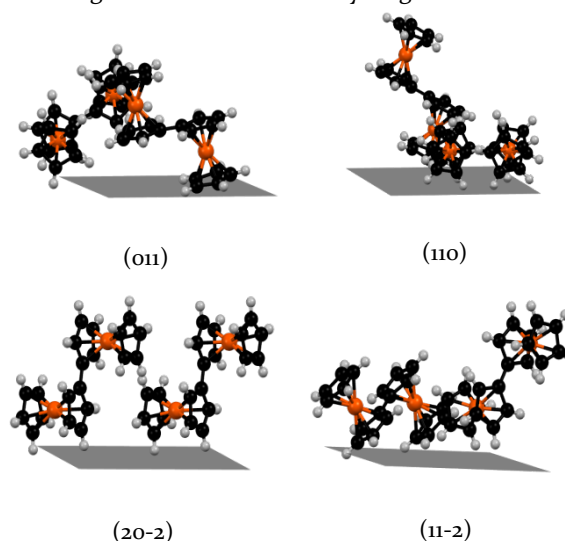

(011)

(110)

(20-2)

(11-2)

Figure 4 Orientation of the biferrocene molecules relative to the substrate plane for the most pronounced XRD peaks.[24]

3.1. Effect of deposition rate on film growth

As seen in Figure 1, higher deposition rates resulted in higher film coverages with an increase from 30 ± 13% to 35 ± 1% on Si, 42 ± 2% to 72 ± 1% on Kapton and 70 ± 2% to

about 81 ± 1% on PTCDA. In the case of biferrocene on Si and Kapton, the increase in coverage also led to an increase in the film thickness equivalent calculated using the total grain volume. The film thickness equivalent increased from 73 ± 33 nm to 112 ± 4 nm on Si and from 161 ± 12 nm to 230 ± 2 nm on Kapton. The higher deposition rate also led to a more uniform coverage, as indicated by the decrease in the values of the standard deviation for the calculated film thicknesses; this was most pronounced on Si, with a decrease from ±13 nm to ±1 nm. The increase in coverage is a sign that for higher deposition rates a lower number of molecules are able to desorb from the surface before diffusing to a nucleation site. Due to the increase of nucleation sites with increasing deposition rate, the ratio between diffusion length λ and average grain spacing σ shifts from $\lambda > \sigma$ towards $\lambda \leq \sigma$. Thus, the number of molecules desorbing from the surface before being incorporated in an existing grain decreases, resulting in a higher coverage. Furthermore, an increase in the nucleation density resulted in a decrease in the average grain and crystal size. A similar deposition rate dependence has been reported for other molecular systems, e. g. ultrathin pentacene films on SiO_2.[26]

XRD measurements, Figure 3, also revealed differences in the crystal structure of biferrocene on PTCDA and Si depending on the deposition rate. Although absolute intensities in XRD patterns should be treated with caution, for all substrates investigated, a clear decrease of the main peak corresponding to the plane oriented along the (110) direction was observed, suggesting a decrease in crystallinity with increasing deposition rate. This observation correlates with the decrease in crystal size seen in SEM, and particularly in the AFM images where smaller grains can be resolved within the islands (Figure 2). In the case of biferrocene on PTCDA, the peaks at $2\theta = 28.68°$ and $2\theta = 29.76°$ corresponding to the (20-4) and the (22-2) planes observed for a deposition rate of 0.1 Å s^{-1} disappeared for higher deposition rates. This can be explained by the initially low intensity of these peaks and the overall decrease in peak intensity at higher deposition rate. No major differences were observed in the case of the diffraction pattern of biferrocene on Kapton. In the case of biferrocene on Si, the peak at $2\theta = 16.31°$ corresponding to the (110) plane decreased significantly with increasing deposition rate from a texture factor of 1.16 to 0.33 and the peak corresponding to the (200) plane disappeared. Furthermore, an additional peak appeared for higher deposition rates at $2\theta = 28.68°$ and became the preferential orientation. Therefore, biferrocene on Si develops the same structure but pronounced differences in texture dependent on the deposition rate. However, no dependencies of this kind were observed on PTCDA.
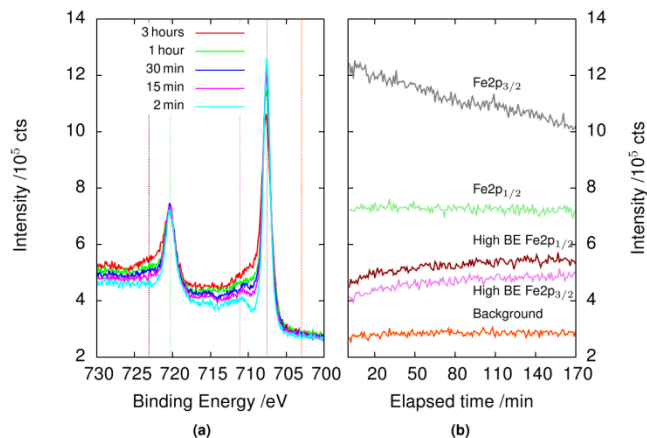
3.2. Chemical characterisation of the thin films

Figure 5 (a) Fe 2p peak of biferrocene was measured for three hours using 6 s scans averaged over two minutes. (b) Behaviour of the Fe 2p peak at key energies (marked by vertical lines in (a)) over time; values are averaged over one minute.

The chemical integrity of the biferrocene thin films was ascertained using XPS and Raman spectroscopy. However, multiple studies conducted on ferrocene have shown that ferrocene is not stable under photon, electron and ion irradiation.[27, 28] Therefore, initial tests regarding the stability of the thin films were carried out by exposing the sample for three hours to the X-ray source and flood gun while monitoring the change in peak shape over time. The results are shown in Figure 5, with Figure 5a showing the Fe 2p peaks after different exposure times and 5b showing the intensity at selected binding energies over time. A linear decrease in peak intensity was observed for the maximum value of the Fe $2p_{3/2}$ peak (707.5 eV). Furthermore, the appearance of an additional component at a binding energy between 708 and 710 eV was observed. Since the film degradation was pronounced enough to be visible by eye, we were able to correlate the size of the degraded area to a spot size of 1 mm in diameter corresponding to the electrons coming from the flood gun rather than the ion spot size of 2 mm in diameter and the X-ray spot size of 400 μm in diameter.

To overcome this difficulty, subsequent XPS spectra were acquired by mapping over the surface with spectra lasting in total less than 30 s being taken in every spot. The spectra taken in 150-200 measurement spots were then averaged to improve the signal to noise ratio.

Figure 6 shows the Fe $2p_{3/2}$ peak of biferrocene on Kapton, PTCDA and biferrocene powder. A binding energy of 707.5 eV for the Fe $2p_{3/2}$ peak of biferrocene powder and biferrocene on Kapton, and 707.4 eV for biferrocene on PTCDA was observed. The measured binding energies are close to previously published values for ferrocene, which lie between 707.3 eV and 707.7 eV[29, 30] and that for biferrocene reported at 707.7 eV.[31]
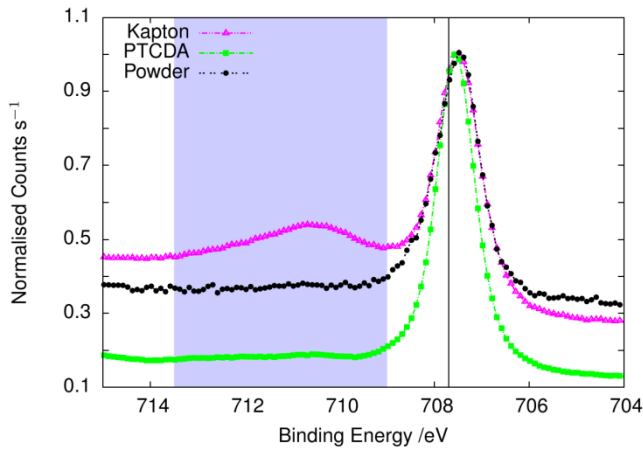
Figure 6 Fe $2p_{3/2}$ peak of biferrocene on Kapton and PTCDA (200 nm, 0.1 Å s^{-1}) and biferrocene powder, spectra are averaged over 160-180 measuring spots. The black vertical line at 707.70 eV represents the previously observed value for the Fe $2p_{3/2}$ peak of biferrocene.[31] The blue shaded area marks the binding energy range identified as being correlated to fragmented Fc_2 molecules.

For the biferrocene thin film on Kapton, an additional Fe $2p_{3/2}$ peak component at higher binding energy was observed. This suggests that a fraction of the biferrocene was modified during or after the deposition process. The ratio between the biferrocene and the impurity component was ≈ 2:1; no additional peak contribution was observed on PTCDA and for the biferrocene powder. The hypothesis that the peak contribution at higher binding energy being a satellite peak was excluded based on the substrate dependence of the peak contribution and the fact that no satellite peak had been previously reported in the literature for ferrocene.[29] The contribution at higher binding energy can be attributed to iron oxides, such as Fe_2O_3 or Fe_3O_4 or a mixture thereof based on the binding energy of the peak component[32-34] and the subsequently presented SQUID measurements.

The main C 1s peak was observed at 284.4 eV, a discrepancy of only 0.3 eV compared to the value published previously for ferrocene of 284.7 eV.[29]

The biferrocene powder and thin films were also characterized using Raman spectroscopy (Figure S1) and show the same vibrational modes with a shift of 0-10 cm^{-1} in comparison to values published for ferrocene. Multiple peaks not previously observed for ferrocene[35] corresponding to vibrational modes of the two ferrocene monomers relative to each other were measured; the most prominent peaks occur at a Raman shift of 433 cm^{-1}, 679 cm^{-1}, 919 cm^{-1}. No peaks related to iron oxides were observed due to the low sensitivity of the spectrometer used.
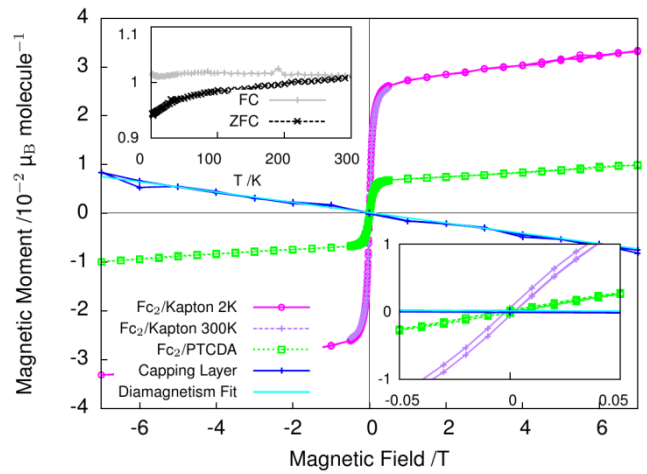
3.3. Magnetic characterisation of the thin films

Figure 7 Magnetic moment in dependence of the applied external magnetic field of biferrocene deposited directly on Kapton (0.1 Ås^{-1}, measured at 2 K and 300 K) and PTCDA (0.1 Å s^{-1}, measured at 300 K) without capping layer and on PTCDA on Kapton (0.1 Å s^{-1}, measured at 10 K) protected from air by a 100 nm LiF capping layer measured using a SQUID. The insert in the upper left quadrant shows the magnetic moment over temperature field cooled and zero field cooled (0.15 Å s^{-1}, measured at 0.025 T). The insert in the lower right quadrant shows the opening of the hysteresis in more detail.

The magnetic properties of the biferrocene thin films were characterized in order to explore possible spintronic applications and to verify the chemical integrity of the biferrocene thin films. As shown in Figure 7, the initial SQUID measurements of biferrocene deposited on Kapton showed weak ferromagnetic behaviour in the 10^{-2} μB/molecule range even at room temperature. The variation of the magnetic moment over a temperature range of 2-300 K showed similarities with ferrimagnetic iron oxide nanoparticles such as Fe_3O_4 and γ-Fe_2O_3,[36, 37] further supporting the chemical assignment from XPS. Initial SQUID measurements on Kapton showed a magnetic moment of about 3 x 10^{-2} μB/molecule, whereas measurements of biferrocene on PTCDA showed a magnetic moment of 1 x 10^{-2} μB/molecule, reduced by a factor of 3 compared to biferrocene on Kapton substrate. This substrate dependence together with the XPS results shows that the oxidation does not occur preferentially on the grain surfaces, but is likely to occur at the biferrocene/substrate interface, following a multistep process as outlined below. The detection of iron oxide for biferrocene on PTCDA in the SQUID measurements in contrast to the XPS measurements can be explained with the high sensitivity of the SQUID to unpaired spins and SQUID being a bulk technique measuring the whole sample volume at once in contrast to the rather small sampling volume of the XPS. However, the substrate dependence of the impurity feature is in both the XPS and SQUID measurements.

Previous studies have shown that capping an air sensitive film with LiF is an efficient way to protect the film from oxidation.[19, 38, 39] Therefore, to mitigate the formation of magnetite impurities, a LiF capping layer was applied to

the biferrocene on PTCDA to protect the film from air exposure. Measurement of the sample protected from air by the capping layer (Figure 7) indeed showed the diamagnetic behaviour expected of biferrocene[4] with a magnetic susceptibility χ of about -2 x 10^{-6} emu T^{-1}. Hence, as schematically shown in Figure 8, we conclude that a fraction of the molecules break up when reaching the substrate with the cyclopentadienyl rings binding to the substrate. Subsequently, the exposed iron atoms react with oxygen upon exposure to air, which can be prevented with a LiF capping layer.[19, 38, 39] This phenomenon is most severe on Kapton, possibly because of the electrostatic charging of the Kapton foil during substrate preparation.[40] A similar break up behaviour was observed for ferrocene during STM studies on graphite[41] and gold.[42] If the breaking up of the biferrocene molecules could be controlled locally via an electron beam or anodic oxidation, it may be possible to write ferromagnetic patterns in the film.
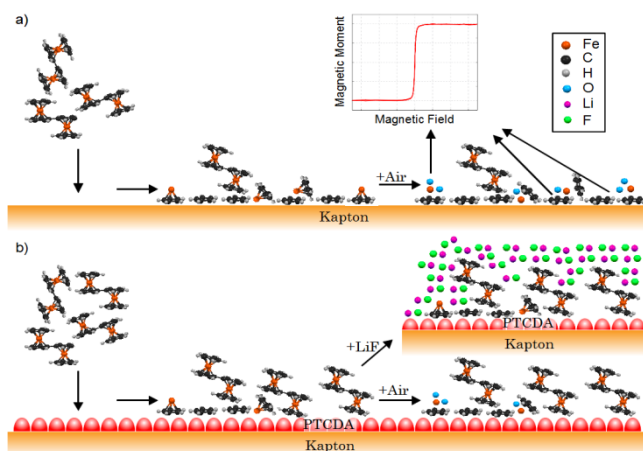

Figure 8 Schematic representation of the breaking up of the biferrocene molecules due to interactions with a) the Kapton and b) PTCDA substrate and subsequent oxidation of the Fe atoms during air exposure.

4. Conclusion

We have demonstrated the successful deposition at room temperature of biferrocene thin films on different substrates via thermal sublimation. Furthermore, a methodology to mitigate the fracturing of biferrocene molecules during the deposition process was developed. This was achieved by using PTCDA as a seeding layer and by capping the thin film with LiF. The chemical integrity of the biferrocene thin films was investigated by XPS and Raman, and its magnetic properties using SQUID. The XPS and Raman data showed good agreement with published literature on biferrocene and ferrocene powder and single crystal. For biferrocene on Kapton in contrast to PTCDA, the XPS measurements showed an additional iron oxide component. The iron oxide was also observed via the ferromagnetic behaviour in the SQUID measurements of biferrocene on Kapton. Furthermore, the SQUID measurements of biferrocene on PTCDA showed the diamagnetic behaviour expected of biferrocene. Additionally, the dependence of the film structure on the substrate and the deposition

rate was investigated. Differences in the nucleation density and grain shape were observed with biferrocene on silicon and Kapton forming few but bigger grains compared to biferrocene on PTCDA due to weak interactions between the substrate and the molecules and biferrocene on PTCDA forming more regular and densely packed grains. Furthermore, it was shown that biferrocene preferentially interacts via H-bonds with all substrates studied. The successful deposition of biferrocene thin films on room temperature substrates, which we expect to be applicable to the bimetallocene family, together with the ability to control the spin *via* oxidation previously observed on microcrystals[11] opens up new avenues for future spintronic applications of such materials.

Furthermore, locally induced breaking up and oxidation of the molecules could be utilised for generating magnetic patterns on the nanoscale.

ASSOCIATED CONTENT

Supporting Information. Raman spectrum of Fc$_2$ thin film and powder and NMR spectra of FcI and Fc$_2$. This material is available free of charge via the Internet at http://pubs.acs.org.

AUTHOR INFORMATION

Corresponding Author

*Email: s.heutz@imperial.ac.uk

Author Contributions

The manuscript was written through contributions of all authors. / All authors have given approval to the final version of the manuscript.

ACKNOWLEDGMENT

REFERENCES

(1) Kealy, T. J.; Pauson, P. L., A New Type of Organo-Iron Compound. *Nature* **1951**, 168, 1039-1040.

(2) Miller, S. A.; Tebboth, J. A.; Tremaine, J. F., 114. Dicyclopentadienyliron. *J. Chem. Soc.* **1952**, 632-635.

(3) Inkpen, M. S.; Sheerer, S.; Linseis, M.; White, A. J. P.; Winter, R. F.; Albrecht, T.; Long, N. J., Oligomeric ferrocene rings. *Nat. Chem.* **2016,** 8, 825-830.

(4) Barlow, S.; O'Hare, D., Metal-Metal Interactions in Linked Metallocenes. *Chem. Rev.* **1997,** 97 (3), 637-670.

(5) Paul, R.; Reifenberger, R. G.; Fisher, T. S.; Zemlyanov, D. Y., Atomic Layer Deposition of FeO on Pt(111) by Ferrocene Adsorbtion and Oxidation. *Chem. Mat.* **2015**, 27(17), 5915-5924.

(6) Mochida, T., Ionic(I)-Ionic(II) Phase Transition in a Biferrocenium Charge-Transfer Complex. *Mol. Cryst. Liq. Cryst* **2007,** 455, (1), 113-116.

(7) Schlesinger, R.; Bianchi, F.; Blumstengel, S.; Christodoulou, C.; Ovysannikov, R.; Kobin, B.; Moudgil, K.; Barlow, S.; Hecht, S.; Marder, S. R.; Henneberger, F.; Koch, N., Efficient light emission from inorganic and organic semiconductor hybrid structures by energy-level tuning. *Nat. Commun.* **2015,** 6, 6754.

(8)   Akaike, K.; Nardi, M. V.; Oehzelt, M.; Frisch, J.; Opitz, A.; Christodoulou, C.; Ligorio, G.; Beyer, P.; Timpel, M.; Pis, I.; Bondino, F.; Moudgil, K.; Barlow, S.; Marder, S. R.; Koch, N., Effective Work Function Reduction of Practical Electrodes Using an Organometallic Dimer. *Adv. Funct. Mater.* **2016**, 26, 2493-2502.

(9)   Rao, C. N. R.; Sen, R.; Satishkumar, B. C.; Govindaraj, A., Large aligned-nanotube bundles from ferrocene pyrolysis. *Chem. Commun.* **1998**, (15), 1525-1526.

(10)   Lee, Y. T.; Kim, N. S.; Park, J.; Han, J. B.; Choi, Y. S.; Ryun, H.; Lee, H. J., Temperature-dependent growth of carbon nanotubes by pyrolysis of ferrocene and acetylene in the range between 700 and 1000 °C. *Chem. Phys. Lett.* **2003**, 372, (5-6), 853-859.

(11)   Hudeczek, P.; Köhler, F. H., Pramagnetic decamethylbimetallocenes. *Organometallics* **1992**, 11 (5), 1773-1775.

(12)   Hilbig, H.; Hudeczek, P.; Köhler, F. H.; Xie, X.; Bergerat, P.; Kahn, O., Ferro- and Antiferromagnetic Exchange in Decamethylbimetallocenes. *Inorg. Chem.* **1998**, 37, 4246-4257.

(13)   Zhou, L.; Yang, S. W.; Ng, M. F.; Sullivan, M. B.; Tan, V. B. C.; Shen, L., One-Dimensional Iron-Cyclopentadienyl Sandwich Molecular Wire with Half Metallic, Negative Differential Resistance and High-Spin Filter Efficiency Properties. *J. Am. Chem. Soc.* **2008**, 130, (12), 4023-4027.

(14)   Matsuura, Y., Spin transport in bimetallocene. *J. Appl. Phys.* **2013**, 114, 103707.

(15)   Matsuura, Y., Current rectification in nickelocenylferrocene sandwiched between two gold electrodes. *J. Chem. Phys.* **2013**, 138, 014311.

(16)   Zeng, J.; Xie, F.; Chen, K. Q., High-efficiency spin-filtering and magnetoresistance effects in supramolecular spin valves. *Carbon* **2016**, 98, 607-612.

(17)   Ormaza, M.; Bachellier, N.; Faraggi, M. N.; Verlhac, B.; Abufager, P.; Ohresser, P.; Joly, L.; Romeo, M.; Scheurer, F.; Bocquet, M. L.; Lorente, N.; Limot, L., Efficient Spin-Flip Excitation of a Nickelocene Molecule. *Nano. Lett.* **2017**, 17, (3), 1877-1882.

(18)   Durston, P. J. Scanning tunnelling microscopy studies of small particles on surfaces. Cambridge University, 1997.

(19)   Heutz, S.; Mitra, C.; Wu, W.; Fisher, A. J.; Kerridge, A.; Stoneham, M.; Harker, T. H.; Gardener, J.; Tseng, H.-H.; Jones, T. S.; Renner, C.; Aeppli, G., Molecular Thin Films: A New Type of Magnetic Switch. *Adv. Mater.* **2007**, 19, (21), 3618-3622.

(20)   Zhang, S.; Zhang, D.; Liebeskind, L. S., Ambient Temperature, Ullmann-like Reductive Coupling of Aryl, Heteroaryl, and Alkenyl Halides. *J. Org. Chem.* **1997**, 62, (8), 2312-2313.

(21)   Inkpen, M. S.; Du, S.; Driver, M.; Albrecht, T.; Long, N. J., Oxidative purification of halogenated ferrocenes. *Dalton Trans.* **2013**, 42, 2813-2816.

(22)   Heutz, S.; Cloots, R.; Jones, T. S., Structural templating effects in molecular heterostructures grown by organic molecular-beam deposition. *Appl. Phys. Lett.* **2000**, 77, (24), 3938.

(23)   Tseng, H. H.; Serri, M.; Harrison, N. M.; Heutz, S., Thin film properties of tetracyanoquinodimethane (TCNQ) with novel templating effects. *J. Mater. Chem. C* **2015**, 3, 8694-8699.

(24)   Solntsev, P. V.; Goetsch, W. R.; Nemykin, V. N., Formation of an Unexpected Organometallic Mercury Compound in a Palladium-Catalyzed Reaction. *Organometallics* **2011**, 30, 6636-6640.

(25)   Barrett, C.; Massalski, T. B., *Structure of Metals: Crystallographic Methods, Principles, and Data*. Pergamon Press Ltd: 1980.

(26)   Pratontep, S.; Brinkmann, M., Correlated growth in ultrathin pentacene films on silicon oxide: Effect of deposition rate. *Phys. Rev. B* **2004**, 69, 165201.

(27)   Welipitiya, D.; Green, A.; Woods, J. P.; Dowben, P. A.;, Ultraviolet and electron radiation induced fragmentation of adsorbed ferrocene. *J. App. Phys.* **1996**, 79, 8730.

(28)   Svensson, K.; Bedson, T. R.; Palmer, R. E., Dissociation and desorption of ferrocene on graphite by low energy electron impact. *Surf. Sci.* **2000**, 451, (1-3), 250-254.

(29)   Connor, J. A.; Derrick, L. M. R.; Hillier, I. H., High Energy Photoelectron Spectroscopy of Transition Metal Complexes. *J. Chem. Soc., Faraday Trans. 2: Molecular and Chemical Physics* **1974**, 70, 941-944.

(30)   Fischer, A. B.; Wrighton, M. S.; Umana, M.; Murray, R. W., An X-ray Photoelectron Spectroscopic Study of Multipayers of an Electroactive Ferrocene Derivative Attached to Platinum and Gold Electrodes. *J. Am. Chem. Soc.* **1979**, 101, (13), 3442-3446.

(31)   Cowan, D. O.; Vanda, C. L.; Park, J.; Kaufman, F., Mixed Valence Ferrocene Chemistry. *Acc. Chem. Res.* **1973**, 6, (1), 1-7.

(32)   Gupta, R. P.; Sen, S. K., Calculation of multiplet structure of core p-vacancy levels. *Phys. Rev. B* **1974**, 10, 71-77.

(33)   Gupta, R. P.; Sen, S. K., Calculation of multiplet structure of core p-vacancy levels II. *Phys. Rev. B* **1975**, 12, 15-19.

(34)   Grosvenor, A. P.; Kobe, B. A.; Biesinger, M. C.; McIntyre, N. S., Investigation of multiplet splitting of Fe 2p XPS spectra and bonding in iron compounds. *Surf. and Interface Anal.* **2004**, 36, 1564-1574.

(35)   Bodenheimer, J. S.; Low, W., A vibrational study of ferrocene and ruthenocene. *Spectrochim. Acta* **1972**, 29A, 1733-1743.

(36)   Goya, G. F.; Berquó, T. S.; Fonseca, F. C.; Morales, M. P., Static and Dynamic magnetic properties of spherical magnetite nanoparticles. *J. Appl. Phys.* **2003**, 94, (5), 3520.

(37)   Pascal, C.; Pascal, J. L.; Favier, F., Electrochemical Synthesis for the Control of $\gamma -Fe_2O_3$ Nanoparticle Size. Morphology, Microstructure, and Magnetic Behavior. *Chem. Mater.* **1999**, 11, (1), 141-147.

(38)   Roldán-Carmona, C.; Malinkiewicz, O.; Betancur, R.; Longo, G.; Momblona, C.; Jaramillo, F.; Camacho, L.; Bolink, H. J., High efficiency single-junction semitransparent perovskite solar cells. *Energy Environ. Sci.* **2014**, 7, 2968-2973.

(39)   Hao-Wu, L.; Si-Wen, C.; Li-Yen, L.; Zheng-Yu, H.; Yi-Hong, C.; Francis, L.; Ken-Tsung, W., Device Engineering for Highly Efficient Top-Illuminated Organic Solar Cells with Microcavity Structures. *Adv. Mater.* **2012**, 24, 2269-2272.

(40)   Lee, J. H.; Jeong, H. C., Removal of static electricity on polyimide film surface by O_2 or Ar cold plasma etching. *Fiber Polym* **2004**, 5, (2), 151-155.

(41)   Durston, P. J.; Palmer, R. E., Adsorbtion and decomposition of ferrocene on graphite studied by HREELS and STM. *Surf. Sci.* **1998**, 400, 277-280.

(42)   Braun, K.-F.; Iancu, V.; Pertaya, N.; Rieder, K.-H.; Hla, S.-W., Decompositional Incommensurate Growth of Ferrocene Molecules on a Au(111) Surface. *Phys. Rev. Lett.* **2006**, 96, 246102.